X-ray diffraction profiling of metal-metal interfaces at the nanoscale

A. V. Darahanau, A. Y. Nikulin,* and R. A. Dilanian
School of Physics, Monash University, Clayton, Victoria 3800, Australia

B. C. Muddle
Department of Materials Engineering, Monash University, Clayton, Victoria 3800, Australia
(Received 10 October 2006; published 15 February 2007)

Several samples containing interfaces between dissimilar metals were examined using diffraction of synchrotron radiation. The complex refractive index profile in the vicinity of the interface for each sample was reconstructed with spatial resolution of about 40 nm by the phase retrieval x-ray diffractometry technique. A series of computer simulations related to the analysis of various configurations of interfaces between dissimilar materials were performed. A practical algorithm of experimental data collection for a detailed examination of internal interfaces was suggested. An estimation of the minimal size of the interface structure modulations, which can be analyzed by the phase retrieval x-ray diffractometry technique, was suggested from the results of computer simulations. It was shown that interface modulations of about 50–100 nm in bimetals can be readily reconstructed by the technique.

DOI: 10.1103/PhysRevB.75.075416 PACS number(s): 61.10.Nz, 68.35.Ct, 42.30.Rx

I. INTRODUCTION

The internal interfaces within a polycrystalline or multiphase material are critical features of the microstructure or nanostructure, with the potential to have a significant influence over both physical and mechanical properties of the material. Indeed, when such interfaces become local zones of microstructural inhomogeneity, or when the scale of the microstructure is reduced to a level at which these interfaces constitute a major proportion of the material volume, then it is the structure and properties of the interfaces, rather than the intrinsic structure and properties of the individual crystals or phases, that dominate control of properties.[1] Similarly, when the film thicknesses in a multilayer device approach the nanoscale, then, regardless of whether the heterolayers are homogeneous or have a structure that is nanoscale, the properties of the assembly are again interface dominated.[2] Given their significance in determining material properties, the characterization of the nature and properties of the interfaces that form between crystalline (and/or amorphous) aggregates that differ in orientation, structure and/or composition has long been a priority.[3] An understanding of these features of such nanostructures is a still greater imperative.[1–5]

When the critical structural dimensions in a material are measured in microns, then optical microscopy combined with conventional x-ray diffraction techniques are sufficient to permit determination of the structure, structural dimensions, and orientation of individual structural domains. When the domains become nanoscale, then such characterization requires high-resolution scanning electron microscopy combined with modern backscattered electron diffraction techniques. However, none of these techniques permit direct characterization of the form, dimensions, and structure of the interfaces between structural domains. For this purpose, the application of high-resolution analytical electron microscopy and diffraction techniques is widespread, but the preparation of suitable thin specimens is destructive of the sample and for the most part limited to orientations for which a selected interface is approximately parallel to the electron beam, and to very limited and highly localized areas of a given interface. The challenge to advancing characterization of such interfaces, and permitting time-resolved *in situ* studies of interface transitions as, for example, a function of temperature or pressure under conditions representative of bulk materials, lies in the development of complementary techniques. The high energy resolution and statistically averaged accuracy of new high-resolution 2D and 3D x-ray diffraction microscopy techniques,[6,7] which use high intensity (synchrotron) x-ray sources, may potentially permit nondestructive characterization of interfaces embedded in macroscopic sections. Unlike early synchrotron x-ray scattering studies of embedded interfaces,[8,9] which were limited to quantitative intensity measurements, the present work uses a highly coherent x-ray source and phase retrieval x-ray diffractometry[10,11] (PRXRD) to map the complex refractive index variation in such interfaces.

In this initial phase of the work, we focus on artificial and macroscopic interfaces created by simple mechanical abutment of dissimilar metals/alloys, in order to demonstrate the hitherto untested extension of this approach into synthesis of the real and imaginary components of the complex refractive index of a material, and the potential of the technique to contribute to the characterization of interfaces between dissimilar metals. It is also necessary to develop practical algorithms of experimental data collection suitable for the detailed characterization of internal interfaces. An estimation of the minimal size of features within interfaces, which can be analyzed by the characterization technique, is also of great importance for further experimental studies.

II. THEORETICAL BASICS OF THE METHOD

In the framework of kinematical diffraction theory, the potential for the examination of non-Bragg diffracting samples using x-ray phase retrieval under Fraunhofer diffraction conditions follows from the variation of the complex

transmission function (CTF) of the sample. The latter describes the interaction between a sample and the incident radiation, and is proportional to the product of its thickness in the direction of incident wave propagation and the complex refractive index[12]

$$t(x) = \exp\left[\frac{2\pi}{\lambda} i \int \{1 - n(x,y,z')\} dz'\right], \quad (1)$$

where $k=2\pi/\lambda$ is the diffraction vector length, $n(x,y,z')$ is the three-dimensional map of the complex refractive index of the material, and z' is the projected thickness of the object in the direction of the incident plane wave propagation z for an ideally monochromatic source of wavelength λ. The complex refractive index is given by $n(x,y,z)=1-\Delta n(x,y,z)=1-[\delta(x,y,z)+i\beta(x,y,z)]$.[13]

The phase-retrieval formalism of the PRXRD technique has been discussed in detail elsewhere.[10,11,14,15] Here we present only the key-steps of the technique, which might be helpful in understanding of the presented results.

The complex diffraction amplitude (CDA), which is an amplitude of the radiation diffracted by an object $R(Q)$ in the case of plane-wave illumination, is a Fourier transform of the complex transmission function $t(x)$:[12]

$$R(Q) = |R(Q)|\exp(i\varphi(Q)) = \int t(x)\exp(2\pi i Q x) dx, \quad (2)$$

where $R(Q)=u(q_r,q_i)+iv(q_r,q_i)$ and q_r, q_i are the real and imaginary parts of the complex scattering vector $Q=q_r+q_i$. The observed diffracted intensity is the square of the modulus of the amplitude $I=|R(Q)|^2$, and thus the phase component of the complex diffraction amplitude and information it contains is lost in experiment.

The PRXRD technique uses the fact that the modulus and the phase of an analytic complex function are not independent, and that the CDA $R(Q)$, and its logarithm $\ln\{R(Q)\}$, are analytic functions.[16,17] By utilizing *a priori* knowledge of the analytical properties of the CDA the phase $\phi(Q)$ of the experimentally observed x-ray diffraction profile can be retrieved from the discrete intensity distribution using a logarithmic dispersion relation[16]

$$\phi(Q) = -\frac{1}{\pi}\wp\int_{-\infty}^{+\infty} \frac{\ln|R(Q')|}{Q'-Q} dQ' + 2\sum_k \arg(Q - Q_k)$$
$$= \phi_{\min}(Q) + \sum_k \phi_k(Q), \quad (3)$$

where Q_k $(k=0,1,2,\ldots,K-1)$ are the true zeros of $|R(Q)|$ in the upper half of the complex plane, and $\wp$ is the Cauchy principle value of the integral. The zeros Q_k of unknown number K, are the true, physical zeros of the CDA that might occur due to interference suppression of the diffracted x-ray wave under certain circumstances.

The second term on the right-hand side of Eq. (3) describes the addition of subsidiary phase due to the presence of "true" zeros of the CDA. Those true, physically meaningful zeros constitute the correct solution (3) of the phase retrieval procedure. However, it is impossible to know *a priori* whether those K true zeros occur in the set of M polynomial zeros of the CDA and their locations. This ambiguity can be resolved by either trial and error method, using *a priori* knowledge about the sample, such as overall size, chemical composition, or shape of the sample,[14] or by utilizing intensity profiles for two different energies of incident radiation.[10,18] The latter method of true zeros localization allows an unambiguous retrieval of the phase of the CDA.[11,15]

Once the true zeros have been identified, the correct profile of CDA can be computed by combining the recorded amplitude profile with the calculated complete phase profile. Using an inverse Fourier transform, it is possible then to obtain the complex transmission function of the sample $t(x)$.[14,15]

The transmission function of the sample is a complex function and its argument and modulus are proportional to the product of the projected thickness and, correspondingly, real and imaginary parts of the complex refractive index. Thus, the reconstruction of the CTF of the sample leaves us with the same uncertainty as in all nontomographic imaging techniques: the ambiguity of the determination of two quantities of interest—thickness and refractive index, from their product

$$|t(x)| = \exp\left\{-k\beta\int dz'\right\} \text{ and } \arg\{t(x)\} = k\delta\int dz'. \quad (4)$$

For a large class of samples with known (or measurable by other means) geometry, the map of the refractive index of the sample can be created, using *a priori* knowledge of the sample dimensions. And *vice versa*, if the sample is homogenous, the profile of the sample thickness variation can be obtained, using *a priori* knowledge of the constant refractive index. If the behavior of both quantities, projected thickness and refractive index, is unknown *a priori*, the problem of sample characterization should be tackled using a tomographiclike approach, similar to the approach demonstrated in one of our previous papers.[15]

Prior experiments related to examination of non-Bragg diffracting samples using the PRXRD technique were focused on the characterization of homogeneous samples, where the analyzed diffraction effects were concerned with the variation of sample geometry (thickness).[14,15,18,19] Thus the more general case of nonhomogenous samples examination, where the diffraction effects are concerned with variations of the complex refractive index or variations of both the thickness and the complex refractive index of the sample, was not experimentally tested. For the case when the thickness of a sample is constant, the variation of the transmission function is determined by the variation of the refractive index across the interface. Thus the form and width of the interface may potentially be determined from the variation in the transmission function as it changes from a constant value for the material on one side of the interface to the constant value for the adjacent material.

Recently, such an experiment with artificially made metal-metal interfaces was performed and results of experimental data analysis were reported.[20] In the present work, the experimental data were reanalyzed using the PRXRD technique

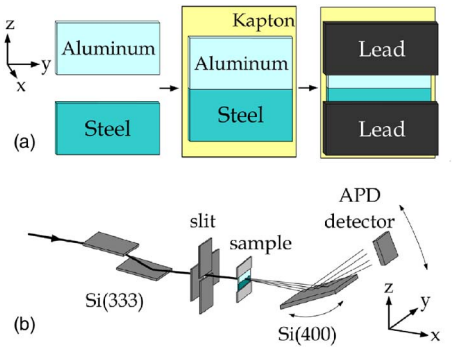

FIG. 1. (Color online) (a) Schematic diagram of sample preparation and (b) experimental setup diagram for the collection of Fraunhofer diffraction profiles at the BL29XU beamline, SPring-8, Japan.

combined with the recently developed Neural Network Root Finder (NNRF) algorithm.[21] The NNRF algorithm allows the calculation of a large number of complex zeros of complex polynomials, and thus allows us to improve the spatial resolution achievable in the structure analysis using the PRXRD technique. In this paper we present the results of experimental analysis of artificially made metal-metal interfaces with the improved resolution. A more detailed consideration of the possibility of nonhomogenous samples examination is presented. An estimation of a minimal size of features within internal interfaces in bimetals which can be analyzed by the PRXRD technique is suggested.

III. EXPERIMENTAL RESULTS

Two sets of samples were prepared for the experiment. The general-purpose 50 μm thick sheets of metals were used for sample preparation. For each sample two strips of different metals (aluminum and steel for the first set, and aluminum and brass for the second set) were cut from 50 μm thick sheets and the planar surfaces placed on a polyimide (DuPont Kapton®) slide with the strips abutted together edge-to-edge to create a straight, planar interface. Contact surfaces were not specially conditioned and thus the interfaces were relatively rough. Given the focus on characterization of the metal-metal interface, each sample was covered by a lead sheet with a small window to expose the interfaces only. That was done in order to eliminate the influence of bulk material on the diffraction data and to simplify the alignment procedure. A schematic representation of the sample geometry is provided in Fig. 1(a).

The experiment was performed at the BL29XU beamline at SPring-8, Japan using the experimental configuration presented on Fig. 1(b). Synchrotron radiation energy of 9.13 keV was selected using a primary, tunable, double-crystal Si (111) beamline monochromator. Further angular collimation was performed using a double-crystal channel-cut Si (333) monochromator placed in asymmetric mode. Then the beam was spatially collimated by two pairs of slits defining a 200 μm horizontal separation and an approximately 20 μm vertical separation. The sample was placed downstream immediately beyond the slits in such a way that the interface between the metal strips was aligned parallel to the horizontal slit and the x-ray scattering diffraction from it occurred in the vertical plane coinciding with the diffraction plane of the x-ray optics. The interface was placed into the beam by scanning the sample over the slit in vertical direction. A Si (400) crystal analyzer and avalanche photo-diode detector, counting in single photon mode, were placed downstream from the sample to collect the diffracted intensity from the metal-metal interface as a function of the angular position of the analyzer. The experimental intensity profiles recorded from the aluminum-brass and aluminum-steel interfaces are presented in Fig. 2(a). An angular range for the analyzer crystal of ±0.1° about the exact Bragg position with a step of 0.0002° were used in the analysis to allow the mapping of the refractive index over 20 μm with a spatial resolution of 40 nm. The methodology of PRXRD (Refs. 10, 11, 14, and 15) in combination with the recently developed algorithm of complex polynomial zeros calculation [Neural Network Root Finder (NNRF)][21] was applied to the analysis of the experimental data. The reconstructed profiles for the real components of the refractive indices for the aluminum-steel and aluminum-brass samples are presented in Fig. 2(b). The use of NNRF algorithm allowed improving the spatial resolution in the reconstructed profiles from 80 nm (reported in Ref. 20) to 40 nm.

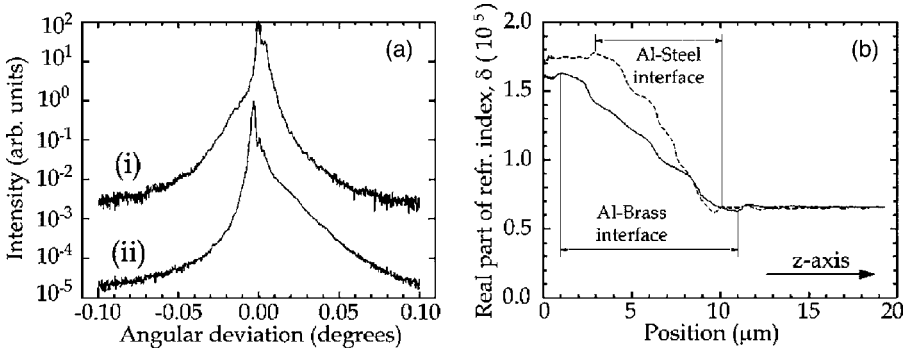

FIG. 2. (a) Experimental Fraunhofer diffraction profiles as a function of analyzer crystal angle from (i) aluminum-brass sample and (ii) aluminum-steel sample. The intensity profile from aluminum-brass sample is shifted up by two orders of magnitude for better visibility and (b) the reconstructed profiles of the real part of refractive indexes for aluminum-steel sample (dotted line) and for aluminum-brass sample (solid line). The origin of the plot corresponds to an edge of the vertical collimating slit.

It is necessary to note that although further improvement of the spatial resolution in the analysis is theoretically possible, from a practical point of view it is restricted by insufficient precision and quality of instrumentation. An experimentally recorded intensity pattern includes not only diffraction effects from the sample of interest, but also diffraction effects from all the objects (and their features) along the path of x rays from the source to the detector. Thus, features of the elements of experimental setup, such as nanodefects of the perfect crystal optics and nanoroughness of the edges of the limiting aperture, etc., will contribute to the formation of the recorded experimental diffraction data. The latter element, i.e., collimating slit, is the most apparent source of unwanted effects,[22] since usually the edges of slit leaves are not specially conditioned. It means that further improvement of the spatial resolution is meaningful only if the surface of the slit edges were specially conditioned to have the size of surface imperfections lesser that the desired spatial resolution. A more detailed consideration of the problem of the collimating slit in relation to the analysis of nanoscale structures will be presented elsewhere. The roughness of the collimating slit edges in this experiment was estimated in the range of 30–50 nm, and thus further improvement of the spatial resolution in experimental data analysis would be meaningless.

Since the experimental data were recorded at one incident radiation energy, the "trial and error" method of zeros localization was applied to determine the set of "true" zeros. The "true" zeros were included in the complete phase profile of the complex diffraction amplitude and this function was inverse Fourier transformed to calculate the complex transmission function (CTF) $t(x)$. The latter is proportional to the product of the complex refractive index and the thickness of the sample in the direction of x-ray propagation.[23] Knowing the thickness of the sample (it was made of 50 μm thick metal strips), it was possible to map the distribution of complex refractive index within the irradiated fragment of the sample. The phase profile of the reconstructed transmission function is proportional to the variation of the real part of the complex refractive index and the modulus corresponds to the variation of the imaginary part of the complex refractive index, as in Eq. (2).

Since the phase changes within the diffracted wave can only be retrieved to within an unknown constant,[24] only the relative variation in phase is meaningful. It is seen in Fig. 2(b), both profiles contain the region where the refractive index changes from values for one material $[n_1=1-(\delta_1+i\beta_1)]$ to the other $[n_2=1-(\delta_2+i\beta_2)]$. The minimum level of the reconstructed profile was set to be equal to the real part of the refractive index of aluminum, as we were interested in characterization of the interfaces, rather than determination of materials forming it. The determination of the absolute value of the real part of refractive indices is also feasible in the same experiment, if a set of additional wedge-shaped samples was prepared.[22] For the aluminum-brass sample, the real component of the refractive index changes from $\delta_1=1.62\times10^{-5}$ to $\delta_2=0.65\times10^{-5}$ over a ~10 μm interval, while for the aluminum-brass sample the corresponding change is from $\delta_1=1.75\times10^{-5}$ to $\delta_2=0.65\times10^{-5}$ over a ~7 μm interval. The imaginary components of the refractive indices obtained through the reconstruction showed similar variations in profile as the real components. The complex refractive indices expected theoretically for the materials were $\Delta n=(-0.6560\times10^{-5},0.9499\times10^{-7})$ for aluminum ($Al_{100\%}$), $\Delta n=(-1.8045\times10^{-5},0.18829\times10^{-5})$ for steel ($Fe_{99\%}C_{1\%}$), and $\Delta n=(-1.6850\times10^{-5},0.18303\times10^{-5})$ for brass ($Cu_{60\%}Zn_{40\%}$). The reconstructed refractive index profiles are thus in good agreement with those expected theoretically. The widths of the interfaces were estimated to be ~7 μm for the aluminum-steel sample and ~10 μm for the aluminum-brass sample. The reconstructions presented above showed that the variation of the complex refractive index within a sample is analyzable and, consequently, the proposed approach is valid for the direct, non-destructive characterization of boundaries between different materials.

The characterization of the shape of metal edges forming the interface from a single data set is possible only if there is no overlapping of the metal edges, and thus each part of the sample can be described by the product of the thickness and the refractive index of the corresponding metal. The transmission function of the interface formed by overlapping metals is proportional to a combination of the products of the refractive indices and the thicknesses of metals in the direction of x-ray propagation, where contribution from each metal (thickness of each) is unknown. In order to determine the shape and orientation of the edges of the materials forming the interface, at least two data sets recorded from different orientations of the sample in respect to the incident x rays should be utilized. Ideally, the experimental data should also be collected for two different energies of incident radiation, in order to be able to apply the "two-energy" method of "true" zeros localization in the phase reconstruction routine.[10,11] The application of the "two-energy" method allows one to simplify the procedure of zeros localization, and to ensure the uniqueness of the obtained results.[10]

IV. SIMULATIONS

A series of simulations were executed to test the robustness of the phase retrieval procedure applied to simulated data for various configurations of metal-metal interfaces. It was desirable to understand how varying parameters of the sample and/or experimental setup affect the diffraction data.

The refraction and absorption contrast introduced by the sample to the incident wave were simulated. Here by the "sample" we understand a part of the sample in the vicinity of the interface between two metal pieces illuminated by the radiation passed through an aperture placed just before the sample, as was the case in the aforementioned experiment. The sample was simulated to be aligned in such a way that the interface between the metals was perpendicular to the plane of diffraction (x-z plane in Fig. 1). For convenience, a quasiplane wave incident on an object having a constant refractive index distribution in the y direction was considered. Normal incidence of x rays on the sample was assumed and thus the path length through the object was taken as the thickness of the sample in the direction of the incident x-ray beam propagation. Both metal parts outside the interface were simulated to be 50 μm thick parallel plates. A variety

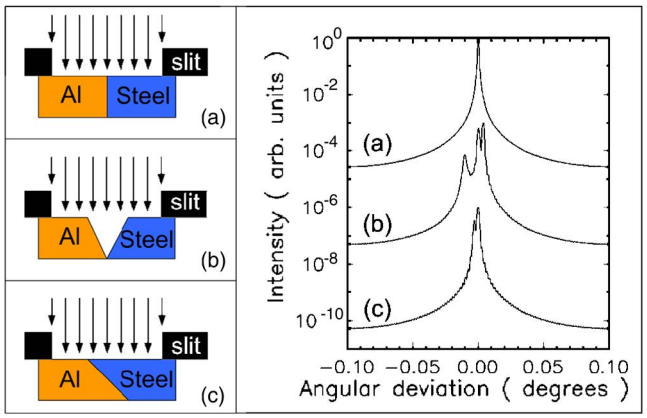

FIG. 3. (Color online) Diagrams of simulated shapes of aluminum-steel interface and corresponding simulated intensity distributions.

of shapes of metal edges forming the interface were simulated with the total thickness of the sample not exceeding 50 μm in that region.

The thickness profile of each piece was combined with the complex refractive index of the corresponding metal at an x-ray energy of 9.13 keV (energy used in the experiment). Then, the complex transmission function (CTF) of the sample was created for each desirable profile of the interface, in accordance with Eq. (1). The simulated complex transmission function was used as the wave incident on the crystal analyzer [Si (400) in Fig. 1(b)]. The reflection of that wave from the crystal-analyzer was calculated using Takagi equations[25] in order to simulate the diffraction pattern from each of the sample configurations under Fraunhofer diffraction conditions. The simulated interval of the sample's surface (in the x direction) and the number of points in simulations were chosen to give the same angular range and step in reciprocal space as they were in the experimental data sets.

Analysis of the simulated intensity profiles was twofold: first, varying the shape and relative positions of the metal edges of the simulated interface, an attempt was made to obtain a diffraction pattern similar to the experimentally observed one. Second, applying the same phase retrieval routine, as was applied to the analysis of the experimental data, we tried to develop algorithms for the mapping of the complex refractive index of various shapes of the simulated nonhomogenous sample.

In general, various shapes of the simulated interface can be grouped into two main categories: single v-butt joint [diagram (b) in Fig. 3] and bevel joint of metal pieces [diagram (c) in Fig. 3]. All the variations of the metal joints could be assigned to one of these categories, as the cumulative path length of x rays through each metal is important for simulations of the complex transmission function of the sample. The borderline case of an ideal square butt joint of metal edges [diagram (a) in Fig. 3] was distinguished since the analysis of such configuration differs from all other cases.

The fine structure of the metal edges which formed the interface roughness was not considered at this stage. A possible influence of the interface roughness on final results is the shift of the profile of the modulus of the CTF. However, this shift is not important in profiling of the structure, as only the relative variations of thickness/refractive index is of importance. The reconstructed by the PRXRD profile of the argument of the CTF is not affected by any presence of imperfections/roughness, as it was discussed in a previous publication.[26]

A. Square butt joint of metal edges

The consideration of the case of a square butt joint of metal edges was of interest for better understanding of the relationship between the measurable in an experiment intensity distribution and the properties of the sample. In such a situation, the complex refractive index of the sample changes steplike within the interval between the two adjacent points, producing an infinite gradient in phase of the diffracted radiation. In practice, the reconstruction of the phase of a wave diffracted from such an object is problematic. If the difference of the refractive indices and the thickness of the sample are sufficient to produce a phase incursion greater than 2π, then the multiples of 2π will be lost and the phase will be represented by a remaining fraction of 2π. The uncertainty of the phase determination can thus lead to incorrect results of the structure examination. This can be illustrated by the following example.

The CTF of the steel-aluminum sample was calculated in accordance with Eq. (1). The refractive indices used in the simulations were $\Delta n(\mathrm{Al})=(-0.6560\times10^{-5},0.9499\times10^{-7})$ and $\Delta n(\mathrm{steel})=(-1.8045\times10^{-5},0.18829\times10^{-5})$. Knowing the thickness of the sample, the profiles of the real and imaginary parts of the complex refractive index of the sample were created from the phase and modulus of the simulated CTF. They are presented in Figs. 4(a) and 4(b), correspondingly. As seen in the figure, the values of the imaginary parts of refractive indices corresponding to aluminum and steel parts of the sample were correctly calculated from the CTF. The difference between real parts of refractive indices is significantly lower than it was postulated in the simulation of the CTF. This means that the phase difference produced by aluminum and steel parts of the sample was greater than 2π. Due to 2π periodicity of the phase function, the multiples of 2π were lost in the reconstructed profile. This resulted in a smaller difference (calculated from the CTF) between the real parts of the complex refractive indices for the two different parts of the sample.

The simulated diffracted intensities from the steel-aluminum and brass-aluminum samples showed that the differences in the complex refractive indices of materials and thicknesses of the samples are so significant that the edges of the heavier materials in both samples served as an edge of the slit. The simulated intensity distributions produced a $\sin c$ function with a period corresponding to the length of the aluminum part of the sample. The period of the fringes varied with the change of the joint position within the simulated aperture and always corresponded to the length of the aluminum part of the sample. The same algorithm of PRXRD technique, as used for the experimental data analysis, was applied to the simulated intensity profile to reconstruct the complex transmission functions of the samples. The recon-

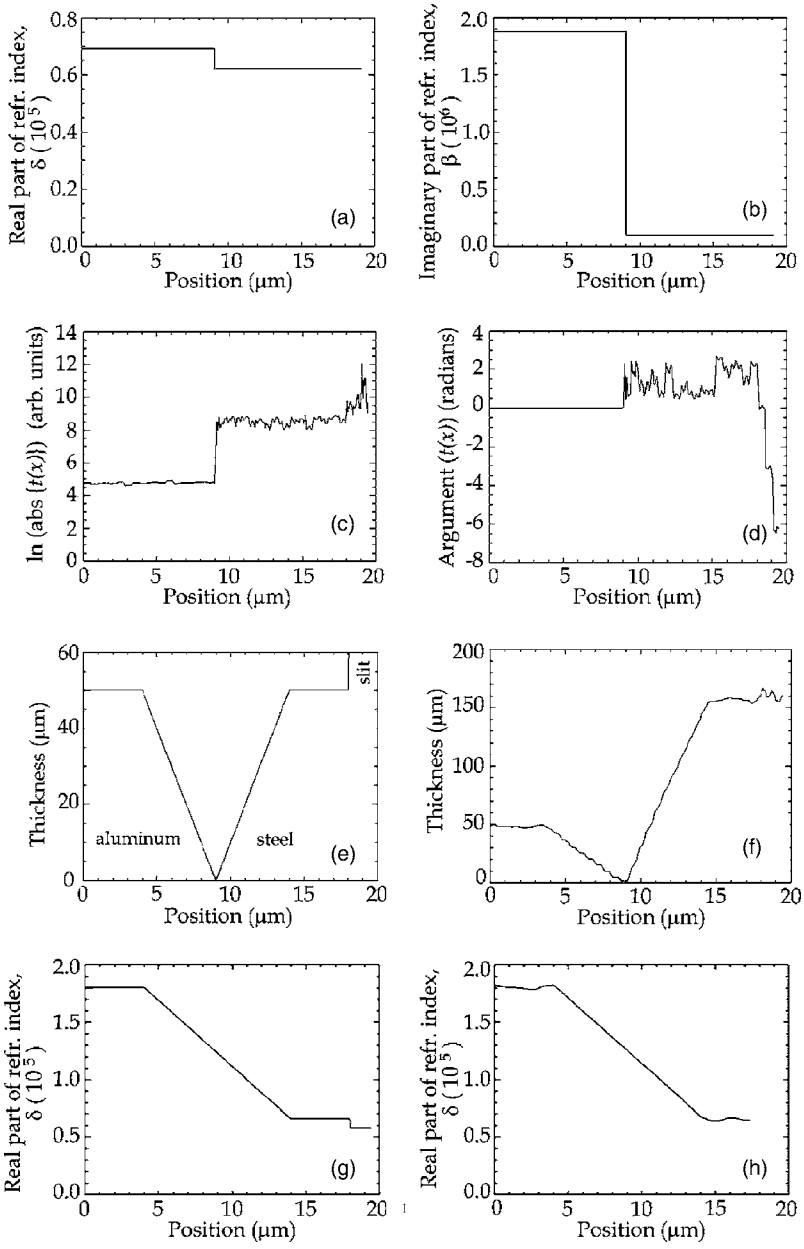

FIG. 4. (a) and (b) Profiles of real and imaginary part of the complex refractive index calculated from the simulated CTF of steel-aluminum sample with square butt joint of metal parts. The discrepancy of calculated and initial values of real part of the refractive indices is a result of multiple 2π loss in the phase of the complex transmission function. (c) and (d) Reconstruction by PRXRD algorithm profiles of modulus and phase of the CTF of the simulated aluminum-steel sample with squared butt joint of metal pieces placed in the middle of 18 μm aperture. (e) and (f) Modeled thickness profile of the v-butt joint of steel and aluminium metal pieces within 18 μm aperture and reconstructed thickness profile of the sample with the assumption that the whole sample has a refractive index of aluminum. (g) and (h) The refractive index profile (real part) of the modeled bevel joint of aluminum and steel metal pieces within 18 μm aperture and reconstructed by PRXRD technique profile of the real part of refractive index of the sample.

structed modulus and phase of the complex transmission function of one of the simulated samples are presented in Figs. 4(c) and 4(d), correspondingly. It is seen in both profiles, that the part corresponding to the steel side of the sample was reconstructed in a fashion resembling a region outside an edge of an aperture.[14] The problems associated with the characterization of a square butt joint when illuminated by a beam parallel to the joint surface can be solved if the sample is slightly rotated with respect to the incident beam. The rotation of the sample changes the problem to the case of a simple bevel joint, described below.

B. V-butt joint of metal edges

The case of a v-butt joint between metals [Fig. 3(b)] is relatively simple for the analysis. The CTF of such interface can be divided into two spatially separated parts. The thickness of both metal parts decreases gradually towards the point of contact. The procedure of the phase reconstruction in this case does not suffer from the loss of a multiple number of 2π, since the phase incursion takes place over a certain length interval. Thus its change is detectable by the reconstruction routine. The variations of the CTF are produced by the changes of the thicknesses in both parts and, thus the shape of the metal edges, forming the interface, can be analyzed directly from the reconstructed CTF profile. It is impossible to predict where the point of connection will be reconstructed in real experimental data analysis. Thus, the thickness profile of the sample should be constructed from the obtained CTF profile with an assumption of the constant refractive index for the whole sample. The choice of the reference refractive index is not important. However, it is preferable to use the one with lower values of the real and imaginary parts. This choice simplifies the correct determination of the contact point position. Since the reconstructed

thickness of a denser part of the sample will have a higher value than in reality, such a choice improves the visibility of the point of connection. After the point of contact is found, the refractive index of the part with incorrect thickness can be changed to the corresponding value to obtain the correct thickness profile.

An example of the reconstruction of a v-butt joint thickness profile from the simulated profile presented in Fig. 4(e) is shown in Fig. 4(f). The profile in Fig. 4(f) was created from the reconstructed profile of the CTF with an assumption of the constant refractive index for the whole sample. It is seen that the reconstructed thickness of the flat part of the right side of the sample has a thickness which is about 2.8 times greater than the thickness of the left one. This number corresponds to the ratio of the real parts of refractive indices of steel and aluminum, which was 2.78 in model profile, and thus after the correction of the refractive index for the right side, the thicknesses of flat regions of metals are equal, as it was modeled. The point of connection between two metals is readily observable and the procedure of the refractive index correction of that part of the profile is straightforward.

Figure 3(b) shows a typical intensity distribution from a v-butt joint between the steel and aluminum metal pieces (joint between brass and aluminum produces a very similar distribution as the values of the refractive indices of steel and brass are close to each other). It can be seen that two wedge metal edges of the sample produce additional (satellite) peaks in the intensity distribution on each side of the central peak, which corresponds to the unrefracted part of the incident beam. The intensity of the peak corresponding to the radiation refracted from the steel edge (right peak in the figure) is higher than the intensity of the central peak. This peak can be misinterpreted as the central one in the analysis of experimentally recorded diffraction data. Such misinterpretation of the position of the central peak can lead to an incorrect solution of phase retrieval and, consequently, incorrect CTF reconstruction.

For the case of v-butt joint with wedge-shaped edges of the metals, the angular positions of satellite peaks with respect to the central one are determined by $\Delta\theta = \delta \tan \varphi$, where δ is the real part of the complex refractive index and φ is the wedge angle of the corresponding metal edge.[22] Thus, the choice of one of the satellite peaks as the central one in the phase retrieval procedure makes the angular distribution of intensity peaks different from that, corresponding to the actual structure (and shape) of the sample. In this case the phase reconstruction algorithm produces an incorrect solution, which corresponds to a structure, the intensity distribution of which has two peaks on one side of the central peak. Obviously, the reconstructed profile of the CTF will be incorrect. Having minimal *a priori* information about the interface configuration or about the thickness of the sample outside the interface, misinterpretation of the central peak can be detected and corrected at early stages of the data analysis.

It is necessary to note, that in an actual x-ray diffraction experiment the situation when the intensity of the central peak is lower than that of satellite peaks, or when the intensity distribution "loses" its prominent central peak, is possible, especially in experiments utilizing a very narrow (5–10 μm) collimating slit.[22] Thus, strong emphasis should be given to the correct determination of the central peak (the origin of the Fourier transform) in the phase retrieval procedure of experimental data analysis.

C. Bevel joint of metal edges

The case of a bevel joint of two metals [Fig. 3(c)] is the most interesting case of the interface configuration in the view of practical nondestructive analysis of interfaces between different materials. In such situation, the sample consists of two parallel-sided plates of metals of the same thickness, which have lapped ends, but the overall thickness of the sample in the region of the interface remains equal to the outer thickness of metal pieces. The CTF of the sample can be divided into three different parts: two regions on each side of the interface where CTF is proportional to the product of the complex refractive index and the thickness of corresponding metal, and the region of the interface where the CTF is proportional to the sum of products of thicknesses and refractive indices of two metals forming the interface. Thus, in the region of the interface, variable thicknesses of lapping metal edges produce a continuous variation of the complex refractive index of the sample from the value corresponding to one metal to the value of another one. The overall thickness is constant throughout the sample and thus, from the reconstructed CTF it is possible to obtain the map of the complex refractive index of the sample. The map of the real part of the refractive index of a model sample and the reconstructed map of the real part of the refractive index are presented in Figs. 4(g) and 4(h), correspondingly.

The CTF of the sample in the region of the interface is proportional to the sum of products of the refractive index and the thickness of the metals forming the interface. To characterize the shape of the interface (i.e., shape of the metal edges forming the interface), it is necessary to solve a linear equation with two variables—thicknesses of metal edges—for every point along the reconstructed profile. The thickness variation of each of the metal edges forming the interface can be calculated from the reconstructed refractive index profile provided that the sample has constant thickness and has no cavities between the edges. In this case, the thicknesses of metal edges are interdependent and thus the linear equation with two interdependent variables can be solved as described below.

If the overall thickness of the sample is L and projected thicknesses of layers forming the interface are L_1 and L_2. Then, for every point x along the surface of the sample it is possible to write the following two equations:

$$L(x) = L_1(x) + L_2(x),$$

$$t(x) = \exp\left\{-\frac{2\pi i}{\lambda}\left(\int_{L_1} n_1 dL_1 + \int_{L_2} n_2 dL_2\right)\right\} = \exp\left\{-\frac{2\pi i}{\lambda}[n_1 L_1(x) + n_2 L_2(x)]\right\},$$

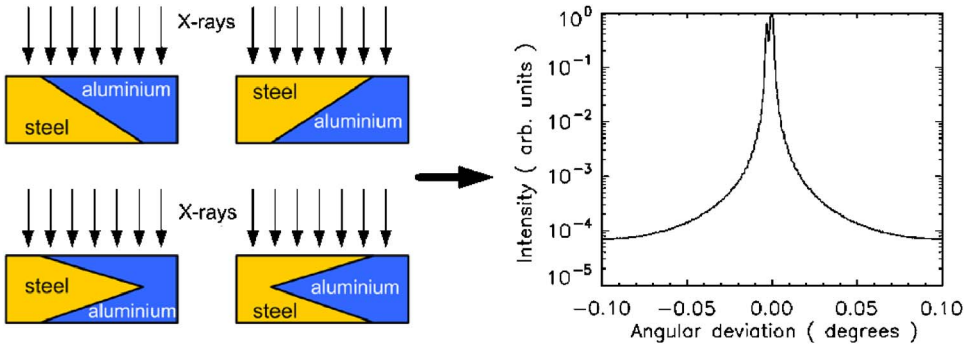

FIG. 5. (Color online) Schematic diagrams of four different shapes of an aluminium-steel interface, having the equivalent projected thicknesses of materials forming the interface in the direction of x rays propagation and simulated intensity distribution of diffracted from any of the interfaces x rays.

where $t(x)$ is the CTF of the sample and n_1 and n_2 are the complex refractive indices of the materials forming the interface.

At every point x in the reconstructed profile of the CTF it is possible to write

$$t_{\mathrm{rec}}(x) = \exp\left(-\frac{2\pi i}{\lambda}[n_{\mathrm{rec}}(x)L(x)]\right).$$

Knowing the overall thickness of the sample one can create the profile of the refractive index of the sample (real and/or imaginary part of it), as follows:

$$n_{\mathrm{rec}}(x) = \frac{n_1 L_1(x) + n_2 L_2(x)}{L(x)},$$

and taking into account the interdependence between L_1 and L_2, the profiles of the projected thicknesses of layers forming the interface can be calculated as

$$L_2(x) = \frac{n_{\mathrm{rec}}(x) - n_1}{n_2 - n_1}L(x), \quad L_1(x) = \frac{n_2 - n_{\mathrm{rec}}(x)}{n_2 - n_1}L(x).$$

The CTF of the sample is proportional to the product of the complex refractive index and the thickness of the sample in the direction of incident wave propagation.[23] Consequently, different configurations of an interface with the same ratio of overall thicknesses of different materials forming the interface in the direction of wave propagation produce the same CTF and thus, produce the same intensity distribution of the diffracted radiation, as presented in Fig. 5. The overall thicknesses of materials can be reconstructed by the PRXRD technique, but different orientations and shapes of the joint are indistinguishable from the analysis of a single projection data (in this case—normal incidence of x rays on the sample surface). Profiles of the overall thicknesses of materials are different for each certain orientation of the sample in respect to the direction of x-rays propagation, and hence each configuration of the sample has a unique CTF (and thus CDA) as shown in Fig. 6. The analysis of CTF reconstructions for different orientations of the sample with respect to the incident radiation provides enough information to characterize not only the size of the interface and overall thicknesses of materials forming the interface, but also the orientation and geometry of the interface. This can be illustrated by the analysis of two refractive index profiles reconstructed for different projections of the interface of triangular shape, presented in Fig. 6(c).

For each of the projections it is possible to reconstruct the profile of the refractive index. The procedure of the interpretation of multiple projections from the sample is more geometry than physics. The reconstructed profile of the refractive index obtained from a projection when the surface of the sample is perpendicular to the direction of the beam (first projection) will have one interval of refractive index change from the value of one material to the other [similar to the one presented in Fig. 4(h)]. From this projection it is possible to calculate the thicknesses of the materials that form the interface for every point along the (as described above). However it is impossible to determine what was the shape and orientation of the interface, since the reconstructed profile of the refractive index is indistinguishable from the profiles reconstructed from any of the interface configurations presented in Fig. 5. Using the reconstructed refractive index profile for the projection when the interface of the sample makes a certain angle γ with the direction of the incident beam (second projection), it is possible to comprehend the geometry and orientation of the interface.

If, for example, the interface is shaped as presented in Fig. 7, a tilt of the sample (Fig. 7) changes the profile of the projected thickness of the sample and thus, the reconstructed

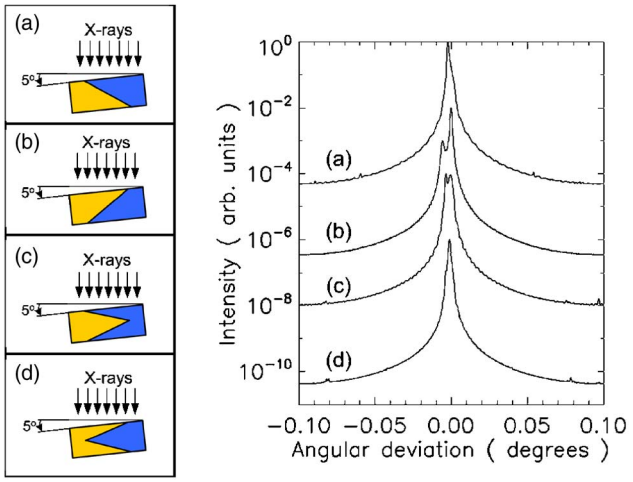

FIG. 6. (Color online) Schematic diagrams of four different shapes of an aluminium-steel interface, having the equivalent projected thickness of materials forming the interface when surface of the sample is perpendicular to the incident beam and corresponding simulated intensity distributions of diffracted from the interfaces x rays in case when surface of the sample make 5° with the normal to the incident beam direction.

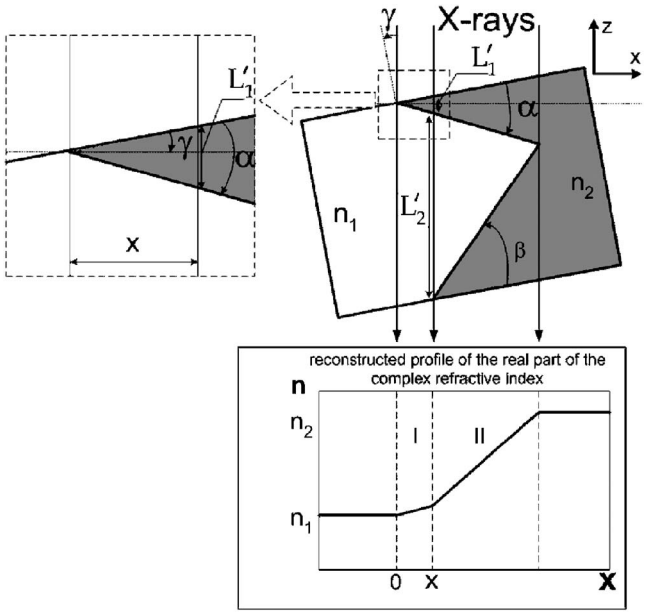

FIG. 7. Schematic diagram of the relationship of the interface geometry with the reconstructed profile of the refractive index.

profile of the refractive index will have a shape which is different from the profile of the first projection. For the second projection, the interval corresponding to the whole area of the interface will split into two intervals with different gradients, as presented in Fig. 7 (intervals I and II in the reconstructed refractive index profile). The projected total thickness of the sample ($L'=L/\cos\theta$) within the interval I consists of two thicknesses of different materials $L'_1(x)$ and $L'_2(x)$. These thicknesses can be calculated using the same algorithm as used for the first projection. Having the thicknesses of metals at the point x and the angle of sample tilt γ, it is possible to calculate the angle α, which is defined as the angle between the upper side of the triangular interface and the upper surface of the sample (see enlarged fragment of the interface in Fig. 7):

$$\alpha = \gamma + \text{arctg}\left\{\frac{[L'_1(x) - xtg\,\gamma]}{x}\right\}.$$

Knowing the angle α, total thickness of the sample and the length of the interface along the surface of the sample (x direction) for the first projection, it is possible to calculate the angle β, which is the angle between the lower side of the triangular interface and lower surface of the sample. And thus, the geometry and the orientation of the interface are determined.

Thus, for a comprehensive analysis of a random interface, the experimental data should be collected using at least two different orientations (stereoprojections) of the area of interest in respect to the incident radiation. For the characterization of more complex interfaces the utilization of multiprojections and further computerized tomographic analysis of projected thickness profiles, similar to the described in Ref. 15, may be necessary.

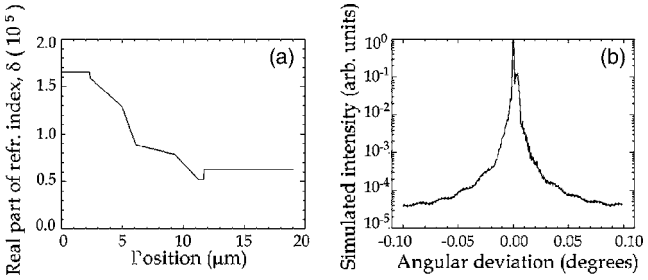

FIG. 8. (a) Simulated profile of the real part of the complex refractive index of the modeled aluminum-brass interface and (b) simulated intensity distribution of x rays diffracted from this model.

It is apparent that the geometry of the interface in the sample used in the experiment was much more complicated than the simulations of simple configurations of metal joints discussed above. The geometry of any real interface in simulations can be represented by using polygonal lines or curves, as only the projection of thickness in the direction of incident wave is important. A series of simulations were performed with the aim to find configurations of interfaces which result in intensity distributions similar to the experimentally recorded ones. One of the possible configurations of the interface along with the corresponding diffraction pattern is presented in Fig. 8. The profiles presented in Figs. 8(a) and 8(b) resemble in appearance the experimental intensity distribution [see Fig. 2(a), profile (i)] recorded from the aluminum-brass sample and reconstructed profile of the complex refractive index for the aluminum-brass sample [Fig. 2(b), solid line].

Usually *a priori* information about the sample structure is very limited and the problem of the reconstruction of a real structure requires the determination of the correct solution from a set of probable solutions. Simulations of complicated profiles of interfaces can help in obtaining additional information about the relationship between the interface configuration and the observable diffraction effects. With an understanding of this relationship, it is possible to conjecture a configuration of the interface that could produce the observed intensity distribution and *vice versa*. It is possible, using computer simulations, to predict what intensity distribution should be observed from a given configuration of the interface. Thus, the simulations of the interfaces can be useful both for obtaining additional information about the sample for the process of its shape reconstruction and for planning of an experiment based on *a priori* information about the sample.

V. MINIMAL SIZE OF FEATURES ANALYZABLE IN INTERNAL INTERFACES

Taking into account the agreement between the experimental results and computer simulations described above, it is possible to conclude that the proposed approach of the PRXRD technique is valid for the nondestructive analysis of internal interfaces. Thus, there is a question: where is the limit of the applicability of the technique or, in other words, what is the minimal size of the features analyzable by the

technique in various samples? From the practical point of view, it is desirable to understand if a technique, which utilizes a conventional x-ray optics, is suitable for the profiling of nanostructures such as embedded interfaces[27] or nanoperiodic surface structures.[28]

A series of simulations were performed with the aim to estimate the minimal size of features analyzable in aluminum-copper and silicon-gold bilayer embedded interfaces. In these simulations the configuration of the sample was different to the samples described above. Here the sample was simulated to have two planar layers—one on top of another. The planar surface of the sample and the interface between dissimilar materials were assumed to be perpendicular to the incident x ray. Thus, x rays were assumed to pass consecutively through the thickness of one material, the interface and the thickness of another material. Outer surfaces of the sample were assumed to be flat (perpendicular to the direction of incident x rays), and thus, the diffraction occurs due to the variation of the thickness of layers that form the interface within the sample. A one-dimensional case was considered, and thus a slice through the sample by an infinitely thin plane, coinciding with the diffraction plane was simulated. The interfaces were simulated to have a periodic triangle shape with period of 1.5 μm and amplitude varying from hundreds to tens of nanometers. Thus, the shape of the simulated interfaces was similar to the shape of the faceted interfaces described in Ref. 27.

The intensity distribution profiles from the samples with embedded interfaces placed behind a 10.2 μm slit were simulated using the same procedure as the aforementioned simulations of the metal-metal interfaces. Symmetric reflections from Si (333) and Si (400) crystal-analyzers were simulated using Takagi equations.[25] The incident x rays were simulated to have energy in the range of 6–18 keV. It was found that the features produced by the interfaces in the diffraction pattern recorded in angular space using simple symmetric reflection from a Si (333) or Si (400) crystal analyzer are the most prominent for x-ray radiation energies of around 9 keV for the aluminum-copper sample and 12 keV for the silicon-gold sample. A possible explanation for this is that those energies are close to the absorption edge of copper (8.98 keV) and gold (11.92 keV), correspondingly.

Gradually reducing the amplitude of the interface structural modulation from several hundred nanometers, it was found that structural variations of about 50–60 nm in silicon-gold and about 80–90 nm in aluminum-copper samples can be readily profiled by the PRXRD technique. A fragment of simulated intensity distribution from an aluminum-copper interface along with the corresponding structure modulation profile mapped by the PRXRD technique is presented in Fig. 9. It is clear that for different configurations of the interface and/or parameters of simulation the estimated numbers might be different. In particular, using a more sophisticated combination of asymmetric reflections from crystal analyzers the diffraction pattern contrast might be improved, making the finer interface modulations analyzable.

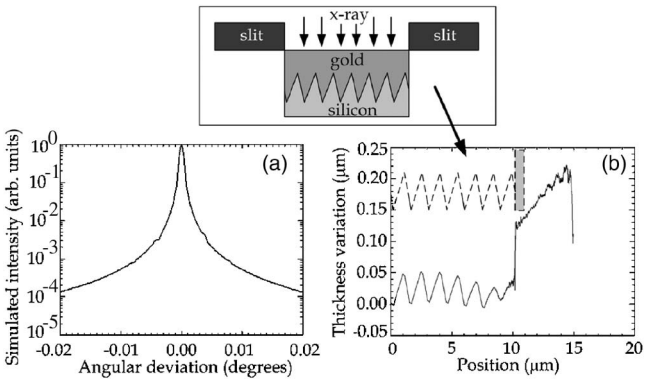

FIG. 9. (a) Diffraction pattern simulated from a modeled faceted interface between silicon and gold, having a periodic triangle shape with period of 1.5 μm and amplitude of variation of 60 nm and (b) thickness variation profile reconstructed by PRXRD technique from the simulated diffraction pattern (solid line) and modeled profile of the interface structure modulation used for simulation of the diffraction pattern (dashed line). The scheme of the modeled sample design is presented in the upper part of the figure.

VI. CONCLUSIONS

This paper reports the results of the experimental analysis of nonhomogenous metal samples using the PRXRD technique. The spatial resolution achieved in the experimental data analysis was 40 nm. It also gives a numerical consideration of the possibility of examination of interfaces between dissimilar materials with submicron resolution using x-ray diffraction. The practical algorithms of experimental data collection and data analysis for some special cases of interfaces were considered. It was shown that for a detailed characterization of internal interfaces between different phases or materials, experimental data should be collected for a number of different projections of the sample with respect to the direction of the incident x-ray beam. In addition to that, experimental data should be collected using two different energies of x rays to ensure the uniqueness of profiling results. The results of simulations showed that the technique might be applicable to the nondestructive profiling of nanoscale variations of structure in embedded interfaces. In particular, for a case of interface between silicon and gold layers, interface structural modulations of about 50 nm were estimated to be analyzable in an experiment utilizing conventional x-ray optics. The experimental evaluation of the reported findings will be performed in the near future.

ACKNOWLEDGMENTS

The Takagi equations codes have been provided by T. Gureyev. The authors acknowledge gratefully the financial support of the Australian Research Council (ARC). One of the authors (A.V.D.) acknowledges the support provided by Monash University.

*Electronic address: Andrei.Nikulin@sci.monash.edu.au

[1] J. D. Embury, C. W. Sinclair, M. J. Mills, H. L. Fraser, A. K. Mukherjee, W. D. Nix, and R. B. Schwarz, Mater. Sci. Eng., A **319-21**, 37 (2001).
[2] C. V. Thompson, Annu. Rev. Mater. Sci. **20**, 245 (1990).
[3] A. P. Sutton and R. W. Balluffi, *Interfaces in Crystalline Materials* (Oxford University Press, Oxford, 1995).
[4] S. P. Baker, M. J. Mills, H. L. Fraser, A. K. Mukherjee, W. D. Nix, and R. B. Schwarz, Mater. Sci. Eng., A **319-21**, 16 (2001).
[5] C. Suryanarayana, Int. Mater. Rev. **40**, 41 (1995).
[6] J. Miao, P. Charalambous, J. Kirz, and D. Sayre, Nature (London) **400**, 342 (1999).
[7] A. Y. Nikulin, O. Sakata, H. Hashizume, and P. V. Petrashen, J. Appl. Crystallogr. **27**, 338 (1994).
[8] D. A. Muller, S. Subramanian, P. E. Batson, S. L. Sass, and J. Silcox, Acta Mater. **44**, 1637 (1996).
[9] S. Subramanian, D. A. Muller, J. Silcox, and S. L. Sass, Acta Mater. **45**, 3565 (1997).
[10] A. Y. Nikulin, Phys. Rev. B **57**, 11178 (1998).
[11] A. Y. Nikulin, Physica B **252**, 319 (1998).
[12] J. M. Cowley, *Diffraction Physics* (Elsevier, Amsterdam, 1995).
[13] R. W. James, *The Optical Principles of the Diffraction of X rays*, edited by L. Bragg (Bell and Sons, London, 1962).
[14] A. V. Darahanau, A. Y. Nikulin, A. Souvorov, Y. Nishino, B. C. Muddle, and T. Ishikawa, Opt. Commun. **251**, 100 (2005).
[15] A. Y. Nikulin, A. V. Darahanau, R. Horney, and T. Ishikawa, Physica B **349**, 281 (2004).
[16] P. V. Petrashen' and F. N. Chukhovski, Sov. Phys. Dokl. **309**, 105 (1989).
[17] N. G. van Kampen, Phys. Rev. **89**, 1072 (1953).
[18] K. Siu, A. Y. Nikulin, P. Wells, E. Harvey, T. Bigault, A. K. Freund, and T. Ishikawa, J. Appl. Phys. **93**, 5161 (2003).
[19] K. Siu, A. Y. Nikulin, K. Tamasaku, and T. Ishikawa, Appl. Phys. Lett. **79**, 2112 (2001).
[20] A. V. Darahanau, A. Y. Nikulin, R. A. Dilanian, B. C. Muddle, A. Souvorov, Y. Nishino, and T. Ishikawa, Appl. Phys. Lett. **88**, 263113 (2006).
[21] R. A. Dilanian, A. Y. Nikulin, A. V. Darahanau, J. Hester, and P. Zaumseil, J. Appl. Phys. **99**, 113526 (2006).
[22] A. Y. Nikulin and J. R. Davis, Opt. Commun. **155**, 231 (1998).
[23] M. Born and E. Wolf, *Principles of Optics* (Cambridge University Press, Cambridge, 2002).
[24] A. Y. Nikulin and P. Zaumseil, Phys. Status Solidi A **172**, 291 (1999).
[25] S. Takagi, J. Phys. Soc. Jpn. **26**, 1239 (1969).
[26] A. V. Darahanau, A. Benci, A. Y. Nikulin, J. Etheridge, J. Hester, and P. Zaumseil, J. Appl. Phys. **99**, 113531 (2006).
[27] T. E. Hsieh and R. W. Balluffi, Acta Metall. **37**, 2133 (1989).
[28] R. A. Wind, M. J. Murtagh, F. Mei, Y. Wang, M. A. Hines, and S. L. Sass, Appl. Phys. Lett. **78**, 2205 (2001).